PCCP

PAPER

Structural characterization of titanium-doped Bioglass using isotopic substitution neutron diffraction

Richard A. Martin,*[ab] Robert M. Moss,[a] Nilay J. Lakhkar,[c]
Jonathan C. Knowles,[cd] Gabriel J. Cuello,[e] Mark E. Smith,[fg] John V. Hanna[f] and
Robert J. Newport[a]

Melt quenched silicate glasses containing calcium, phosphorus and alkali metals have the ability to promote bone regeneration and to fuse to living bone. Of these glasses 45S5 Bioglass® is the most widely used being sold in over 35 countries as a bone graft product for medical and dental applications; particulate 45S5 is also incorporated into toothpastes to help remineralize the surface of teeth. Recently it has been suggested that adding titanium dioxide can increase the bioactivity of these materials. This work investigates the structural consequences of incorporating 4 mol% TiO_2 into Bioglass® using isotopic substitution (of the Ti) applied to neutron diffraction and X-ray Absorption Near Edge Structure (XANES). We present the first isotopic substitution data applied to melt quench derived Bioglass or its derivatives. Results show that titanium is on average surrounded by 5.2(1) nearest neighbor oxygen atoms. This implies an upper limit of 40% four-fold coordinated titanium and shows that the network connectivity is reduced from 2.11 to 1.97 for small quantities of titanium. Titanium XANES micro-fluorescence confirms the titanium environment is homogenous on the micron length scale within these glasses. Solid state magic angle spinning (MAS) NMR confirms the network connectivity model proposed. Furthermore, the results show the intermediate range order containing Na–O, Ca–O, O–P–O and O–Si–O correlations are unaffected by the addition of small quantities of TiO_2 into these systems.

1. Introduction

Bioactive glasses are of great importance due to their ability to chemically bond to bone and stimulate new bone growth.[1,2] Their regenerative potential has been demonstrated in clinical trials and Bioglass®, which has been in clinical use since 1985, has already been used in over a million cases.[3,4] Bioglass®, also known as 45S5, was first reported by Hench and co-workers in 1971 and consists of 45% (by weight) SiO_2, 24.5% CaO 24.5% Na_2O, 6% P_2O_5.[1] Since the development of

Bioglass® there have been many variations on the original composition and form. Numerous ions have been added, or substituted, into Bioglass® to improve properties such as bioactivity and antibacterial effects whilst analogous phosphate-based systems have also been developed.[5–8] In addition, there has been considerable interest in developing sol–gel analogues due to their low processing temperatures and high specific surface area.[9–15] In particular, the atomic-scale structure and network connectivity of these glasses and the effects of these factors on the chemical durability and bioactivity has been the focus of much attention.[16–22] Although there has been considerable interest in the structural chemistry of silicates for decades[23] the addition of an alkali metal, an alkaline-earth metal as well as a second network former in the form of phosphorous means that the generation of a structural model of bioglass is particularly challenging. Whilst significant progress has been made by employing molecular dynamic simulations[16,18,19,24,25] and NMR techniques,[17] relatively few diffraction experiments have been published on the melt-quench derived materials.[26–28]

The present work explores the effect and role of Ti incorporated into melt-quenched Bioglass®. The effect of adding Ti into bioactive silicate glasses is of potential interest for several reasons. Firstly, recent reports have suggested that

[a] *School of Physical Sciences, Ingram Building, University of Kent, Canterbury, CT2 7NH, UK. E-mail: R.A.Martin@Aston.ac.uk*
[b] *School of Engineering & Applied Science and Aston Research Centre for Healthy Ageing, University of Aston, Aston Triangle, Birmingham, B4 7ET, UK*
[c] *Division of Biomaterials and Tissue Engineering, Eastman Dental Institute, University College London, 256 Gray's Inn Road, London, WC1X 8LD, UK*
[d] *WCU Research Centre of Nanobiomedical Science, Dankook University, San#29, Anseo-dong, Dongnam-gu, Cheonan-si, Chungnam, 330-714, South Korea*
[e] *Institut Laue–Langevin, BP 156, F-38042, Grenoble Cédex 9, France*
[f] *Department of Physics, University of Warwick, Coventry CV4 7AL, UK*
[g] *Vice-Chancellor's Office, University House, University of Lancaster, Lancaster, LA1 4YW, UK*

This journal is © the Owner Societies 2012

Phys. Chem. Chem. Phys., 2012, **14**, 15807–15815 | 15807

incorporating Ti into bioactive silicate sol–gels can increase the rate of hydroxyapatite formation.[29] Indeed, Ti is routinely incorporated into bioactive phosphate glasses to control the solubility, improve mechanical properties and also increase bioactivity.[8,30] Cell culture studies have shown Ti phosphate microspheres provide a stable surface for cell attachment, growth and proliferation.[31] However, there have been no structural studies of melt quench derived Ti-doped bioactive silicate glasses.

Secondly, bioactive glasses are routinely used to coat orthopaedic implants made of commercially pure titanium or Ti–Al6–4V.[32] Coating metallic implants with bioactive glass films can improve biological interactions between the bone and the implant and consequently improves adhesion.[33,34] However, bioglass coatings are typically applied using high temperature plasma sprays.[35] Coatings are therefore liable to crack and become delaminated due to the thermal stresses that result from the large differences in thermal expansion between the glass and the metallic implant. Saiz and co-workers reported that even when applying bioactive coatings using a low temperature (820 °C) enameling technique, glasses with less than 60 wt% SiO_2 are prone to cracking and corrosion.[36] Glasses with silica content greater than 60 wt% are more resistant to corrosion and exhibited a lower thermal expansion but showed very poor bioactivity (no hydroxyapatite formation was present even after 2 months in simulated body fluid, SBF).[37] However, titanium silicates are known for their ultra-low thermal expansion. Even relatively low concentrations of Ti can dramatically reduce the thermal expansion of silicates: $(TiO_2)_{0.075}(SiO_2)_{0.925}$ glasses effectively have zero thermal expansion.[38] In addition hydroxyapatite is known to form on Ti–OH functional groups[39,40] which will be formed during the dissolution process of this glass.

Also, from a fundamental perspective, the role of titanium within silicate glasses is of interest because titanium can enter silicate glasses either as a network modifier (6-fold Ti) or a network former (4-fold Ti) where Ti replaces Si. Titanium can also take on a dual role where it enters as a mixture of 4 and 6-fold or as 5-fold (typically a square based pyramid).[41–43] There have been numerous structural studies on titanium-silicate sol–gels and xerogels[44–50] but no studies on melt quench derived titanium-silicate glasses. The coordination of Ti will have a significant effect on the overall network connectivity and the consequent chemical durability under physiological conditions. The ions released from the bioglass will in turn affect, *in vivo*, the biochemical function of proteins.[51,52]

The mechanism of bone formation onto a bioactive glass is a complex multi-step process which has been described by Hench and co-workers.[53] The first stages involve ion exchange of the cations, Na^+ or Ca^{2+}, from the glass with H^+ from the surrounding physiological fluid and the breakage of Si–O–Si bonds to form silanols. The reaction rates of these steps are highly dependent on the overall composition and network connectivity. This is followed by the growth of an amorphous calcium phosphate layer[54] which then crystallizes to form a mixed hydroxycarbonate apatite (HCA) layer.

In order to model and thereby predict the behavior of these materials it is important to have a good understanding of the local structure and the network connectivity, and within that

the environment surrounding the titanium ions. Progress has recently been made on understanding the atomic scale structure of Bioglass® by employing a range of advanced probe techniques including isomorphic substitution neutron diffraction, solid state nuclear magnetic resonance (NMR) and X-ray diffraction thus providing a starting point to model the Ti doped Bioglass.[26–28,55–57]

1.1. Structural model of bioactive glasses

Silicate glasses may be thought of as SiO_4 tetrahedra that are linked by corner-sharing bridging oxygen atoms (O_B). For pure SiO_2, each Si atom has 4 bridging oxygen atoms (each shared by two Si); as additional oxygen atoms are added the SiO_4 tetrahedra remain, but the silicate network is depolymerised through the breaking of Si–O_B–Si bonds. It is therefore useful to describe the network in terms of its connectivity, or Q^n speciation, where Q represents the tetrahedral structural unit and n the number of bridging oxygen per tetrahedra. nQ can vary between 0 and 4, where Q^0 represents orthosilicates, SiO_4^{4-}, Q^4 represents pure SiO_2 and Q^{1-3} represent intermediate silicate structures. For each additional oxygen atom added per 2 Si tetrahedra one bridging oxygen bond breaks to form two non-bridging oxygen atoms (O_{NB}) and Q^n becomes Q^{n-1}.

The chemical durability and dissolution of ions is strongly related to the network connectivity, and bioactive glasses have a typical network connectivity of ~ 2. If the connectivity exceeds ~ 3 the rate of dissolution of ions from the glass (in an aqueous medium such as simulated body fluid, SBF) reduces to the extent that bioactivity ceases.[22] If the network connectivity is too low the glass dissolves too quickly and does not provide either mechanical support, if needed, or the controlled release of ions over a suitably extended time frame (the requirements for which will vary, depending on the context). The connectivity can be controlled by adjusting the ratio of network formers (SiO_2) to network modifiers (such as Na_2O and CaO). The optimum bioactivity for Bioglass is observed to be at 45 weight% SiO_2; compositions in the range 52–60% weight SiO_2 exhibit slower bonding rates and thus lower bioactivity, and glasses with greater than 60% weight SiO_2 are bio-inert.

The network connectivity, NC, is given by

$$NC = 4 - 2Z, \tag{1}$$

where Z, the number of excess oxygen per SiO_2, is given by

$$Z = \frac{c_O}{c_X} - 2 \tag{2}$$

where c_O represents the concentration of oxygen and c_X is the concentration of network formers. The connectivity of Bioglass 45S5 was initially given as 1.90 since it is assumed that the phosphorus enters the glass network and that $Z = [c_O/(c_{Si} + c_P)] - 2$.[22,58] Recent NMR data has however suggested that phosphorus enters the glass as orthophosphate and therefore does not enter the network.[27,28,59] In this case $c_X = c_{Si}$; furthermore, phosphorus can now be considered as a network scavenger, since each P atom is surrounded by 4 oxygen atoms, the number of excess oxygen atoms per SiO_2 is reduced accordingly. Therefore, if phosphorus enters the

glass within an orthophosphate tetrahedron, the number of excess oxygen atoms per SiO_2 is given by

$$Z = \frac{c_O - 4c_P}{c_{Si}} - 2 \qquad (3)$$

In this case $Z = 0.94$, and the network connectivity of glass is equal to 2.11. The increase in network connectivity becomes increasingly important as the content of P_2O_5 is increased.

Ti is a network intermediate and can enter the glass as either a network former (4-fold) or a network modifier (6-fold). Assuming the 4-fold Ti enters the network and does not form phase-separated TiO_4^{4-} units then the excess oxygen per XO_2 unit (where X = Si or Ti) is given by

$$Z = \frac{c_O - 4c_P}{c_{Si} + Rc_{Ti}} - 2 \qquad (4)$$

where R is the fraction of tetrahedral Ti. The initial assumption is justified on the basis of the low molar ratio of $TiO_2 : SiO_2$ which has been fixed at 0.08 : 0.92. Ti : Si ratios of this order have been widely studied in the context of ultra-low thermal expansion materials and is known to consist of a single phase.[42] For the present Ti-silicate system the network connectivity is given by the number of Si–(O)–X bonds per Si where X represent Si or Ti.

2. Experimental

2.1. Sample preparation

Sol–gel derived isotopically enriched titanium silicate $(TiO_2)_{0.08}$-$(SiO_2)_{0.92}$ samples investigated by Pickup et al.[42] were dried overnight at 120 °C to remove any atmospheric adsorbed water before adding the required quantities of sodium carbonate (Na_2CO_3), calcium carbonate $(CaCO_3)$ and ammonium dihydrogen phosphate $(NH_4H_2PO_4)$ to form $(TiO_2)_{3.85}(SiO_2)_{44.3}$-$(Na_2O)_{23.45}(CaO)_{25.9}(P_2O_5)_{2.5}$ (mol%). The powders were mixed thoroughly before transferring into a 90%Pt–10%Rh crucible. The powders were heated at 10 °C per minute to 1370 °C, equilibrated for 90 minutes before pouring onto a preheated (350 °C) graphite mould. These samples were annealed at 350 °C overnight before being allowed to cool slowly to room temperature. The process was repeated for each of the isotopically enriched Ti samples. The density of each sample was measured by helium pycnometry using a Quantachrome Mutlipycnometer. A titanium free bioglass (composition 45S5) was also prepared to act as a control sample.

2.2. Neutron diffraction method and analysis

The neutron diffraction experiments were performed using the D4C instrument at the Institut Laue–Langevin (Grenoble) with an incident neutron wavelength of 0.5 Å.[60,61] The coarsely powdered samples were held at ambient temperature (≈ 25 °C) in a cylindrical vanadium container of 6.8 mm internal diameter and 0.1 mm wall thickness and diffraction patterns were taken for the samples in their container, the empty container and a vanadium rod of dimensions comparable to the sample for normalization purposes. Each complete diffraction pattern was built up from the intensities measured for the different detector groups. These intensities were saved at regular intervals and no deviation between them was observed, apart from the expected statistical variations, which verified the diffractometer stability.[60–62] The program Correct was used to perform the data reduction and corrections.[63,64]

The total structure factor is given by[65]

$$i(Q) = \sum_i \sum_j c_i c_j b_i b_j [\rho_{ij}(Q) - 1] \qquad (5)$$

where c_i and b_i denote the atomic fraction and coherent scattering length of the chemical species i, $\rho_{ij}(Q)$ is the partial structure factor and Q is the magnitude of the scattering vector given by $Q = 4\pi\sin(\theta)/\lambda$ where 2θ is the scattering angle and λ is the incident neutron wavelength. These functions of Q are referred to as reciprocal space data. The corresponding real-space data is obtained by Fourier transforming the total structure factor to give $T(r)$, where

$$T(r) = T^0(r) + \frac{2}{\pi} \int_0^\infty Qi(Q)M(Q)\sin(Qr)dQ \qquad (6)$$

$M(Q)$ is the window function that takes into account the finite experimentally obtainable value of Q ($Q_{max} = 23.66$ Å). $T^0(r)$ is the average density term, given by:[65]

$$T^0(r) = 4\pi r\rho^0 \left(\sum_i c_i b_i\right)^2 \qquad (7)$$

where ρ^0 is the number density. The pair distribution function that results from a neutron diffraction experiment, $T(r)$ can be represented as the weighted sum of partial correlation functions $t_{ij}(r)$.

$$T(r) = \sum_i \sum_j c_i c_j b_i b_j t_{ij}(r) \qquad (8)$$

The coherent neutron scattering lengths $b_{Si} = 4.1491(10)$, $b_{Ca} = 4.70(2)$, $b_{Na} = 3.63(2)$, $b_P = 5.13(1)$ and $b_O = 5.803(4)$ fm were taken from Sears' compilation.[66] The isotopic enrichment of ^{46}Ti and ^{48}Ti were 72.1% and 99.8% respectively, and taking into account the degree of enrichment, the Ti coherent neutron scattering lengths are as follows: $b_{46Ti} = 2.469$ fm and $b_{46Ti} = -6.063$ fm. The negative scattering lengths arise from a π phase shift of the neutron wave function on scattering.

The total interference pattern $i(Q)$ was measured for the ^{46}Ti and ^{48}Ti samples and labeled $^{46}i(Q)$ and $^{48}i(Q)$ respectively. The complexity associated with the number of overlapping correlations in $i(Q)$ can be reduced by forming the first order difference function

$$\Delta i(Q) = {}^{46}i(Q) - {}^{48}i(Q) \qquad (9)$$

The corresponding real space data is therefore given by

$$\Delta T(r) = {}^{46}T(r) - {}^{48}T(r) \qquad (10)$$

It therefore follows that for two glasses identical in every respect apart from the coherent scattering length of the Ti ions, ^{46}Ti and ^{48}Ti, where $b_{46Ti} > b_{48Ti}$, that those correlations not involving Ti will be eliminated. X-ray diffraction, solid state NMR and XANES (X-ray Absorption Near Edge Structure), as well as basic characterization for density and composition, may be used to verify that the samples are indeed identical in all other respects.

Structural information can be obtained by modeling the real-space correlation function. Pair functions $\rho_{ij}(Q)$ are

This journal is © the Owner Societies 2012

Phys. Chem. Chem. Phys., 2012, **14**, 15807–15815 | 15809

generated in Q-space and Fourier transformed to allow comparison with the experimental data in real space. The pair functions are given by:[65]

$$\rho_{ij}(Q) = \frac{n_{ij}w_{ij}}{c_j}\frac{\sin(Qr_{ij})}{Qr_{ij}}\exp\left[\frac{-Q^2\sigma_{ij}{}^2}{2}\right] \qquad (11)$$

where n_{ij}, r_{ij} and σ_{ij} are the coordination number, atomic separation and disorder parameter respectively of atom i in relation to atom j. The weighting factors w_{ij} for a standard neutron diffraction experiment are given by:

$$w_{i\neq j} = 2c_ic_jb_ib_j \qquad (12)$$

$$w_{i=j} = c_i^2b_i^2 \qquad (13)$$

At each stage of the data analysis procedure the reliability of the data was verified. For example, each measured diffraction pattern and difference function should oscillate around the asymptotic expected value and give rise to a well-behaved real-space function: this should oscillate about the calculated low-r limit, and when the oscillations are set to this limit, its back Fourier transform should be in good agreement with the original reciprocal space data set.

2.3. XANES

Titanium X-ray absorption near-edge structure (XANES) data was collected using the micro-focus beam-line I18 at the Diamond Light Source, UK. Spectra were collected from 150 eV below the edge to 135 eV above the edge in order to allow an accurate background subtraction. The spectra were collected in three step sizes; a 5 eV step size was used for the pre-edge (4815–4945 eV), a 0.5 eV step size was used over the pre-peak and edge (4945–5000 eV) and a 1 eV step size after the edge (5000–5100 eV). All measurements were conducted at room temperature. The data was normalized to the incident beam intensity and the spectra were normalized to have an edge step of one. A four micron X-ray spot size was used, several positions on the sample were selected and measured to check uniformity and to confirm that micro-scale phase separation had not occurred.

2.4. ^{31}P and ^{29}Si MAS NMR

^{29}Si MAS NMR data were acquired at 7.05 T using a Varian Infinity Plus-300 spectrometer operating at a characteristic ^{29}Si frequency of 59.61 MHz. All ^{29}Si measurements were single pulse experiments which were implemented using a Bruker 7 mm double-air-bearing probe which enabled magic angle spinning (MAS) frequencies of 5 kHz; $\pi/4$ pulse widths of 4 μs and recycle delays of 30 s were common to these measurements. All ^{29}Si data were externally referenced to kaolinite ($\delta = -92$ ppm). Corresponding ^{31}P MAS NMR data were acquired at 9.4 T using a Bruker DSX-400 spectrometer operating at a characteristic ^{31}P frequency of 161.44 MHz. Single pulse experiments were implemented using a Bruker 3.2 mm double-air-bearing probe which enabled MAS frequencies of up to 20 kHz; $\pi/4$ pulse widths of 1.5 μs and recycle delays of 30 s were common to these measurements. All ^{31}P data were externally referenced to ammonium dihydrogen phosphate ($\delta = -0.95$ ppm).

3. Results and discussion

Three titanium bioglasses were prepared: using naturally abundant Ti, enriched with ^{46}Ti and enriched with ^{48}Ti. These glasses will be referred to as ^{nat}Ti, ^{46}Ti and ^{48}Ti respectively. A fourth titanium-free bioglass (45S5) was also prepared to act as a control sample. The resultant samples were transparent, free from bubbles, and visibly homogeneous. The resultant masses were as expected based on the initial starting mass of the oxides, carbonates and ammonium dihydrogen phosphate allowing for the loss of CO_2, NH_3 and H_2O during the melting procedure. The densities obtained from He pycnometry are 2.70 g cm^{-3} and 2.73 g cm^{-3} for the bioglass and ^{nat}Ti respectively, and the corresponding number densities are and 0.0748 atoms Å^{-3} and 0.0750 atoms Å^{-3}.

The neutron diffraction interference functions, $i(Q)$, for ^{46}Ti and ^{48}Ti are shown in Fig. 1 and the corresponding real space data is given in Fig. 2. The weighting factors w_{ij} formed using eqn (12) and (13) are given in Table 1. As shown, the diffraction patterns are dominated by the oxygen–oxygen correlations ($\sim 40\%$) with the Si–O, Na–O and Ca–O correlations accounting for ~ 16, 15 and 11% of the totals. The Ti–O correlations account for only 1–2% of the diffraction pattern: consequently the Ti–O correlations cannot be directly extracted from the total interference functions. However, since the concentration of Si, Na, Ca, P and O remains constant for all the Ti doped glasses those correlations not containing Ti can be eliminated during the formation of the first order difference function (Table 1).

The first order difference function, $\Delta i(Q)$, formed by $^{46}i(Q)$–$^{48}i(Q)$ is given in Fig. 3 and the corresponding real space information is given in Fig. 4. It can be seen that those correlations not involving Ti have successfully cancelled $e.g.$ the absence of the Si–O and P–O peak ~ 1.6 Å. The difference function is in essence the interference pattern which remains after 98.7% of the data has been subtracted from the total structure factor $^{46}i(Q)$. The first peak (shortest separation in r-space) represents the Ti–O correlation whilst the next nearest
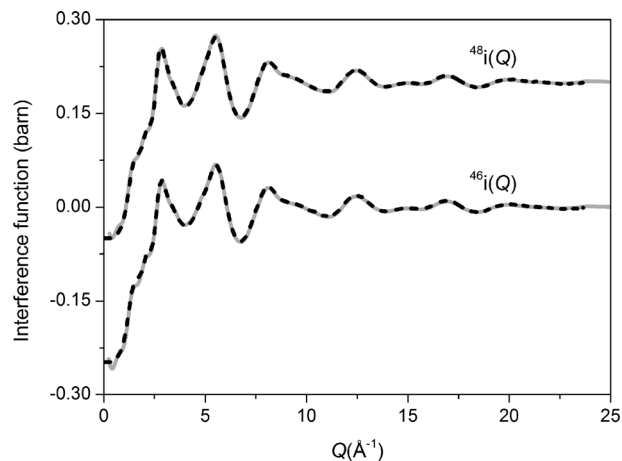

Fig. 1 Total structure factors $^{46}i(Q)$ and $^{48}i(Q)$ for Bioglass doped with ^{46}Ti and ^{48}Ti. The dark broken curve represents the data and the grey curves are the back Fourier transforms of the corresponding $T(r)$ after the unphysical low-r oscillations have been removed. The back Fourier transforms are almost indistinguishable from the $i(Q)$ data points.
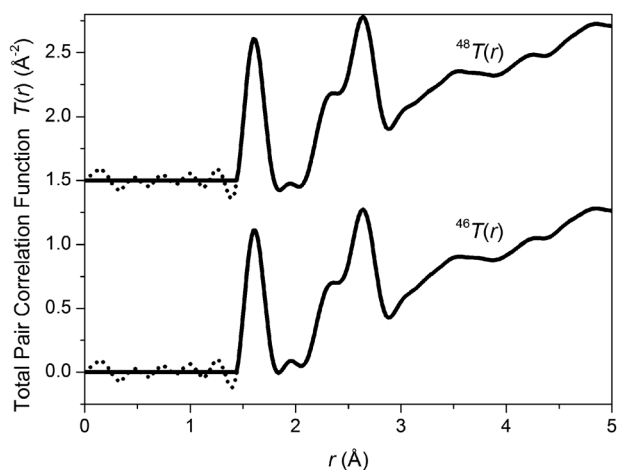
Fig. 2 Real space data $^{46}T(r)$ and $^{48}T(r)$. The broken curve represents the experimental data and the solid curve represents the calculated low-r limit and is used to generate the back Fourier transforms given in Fig. 1.
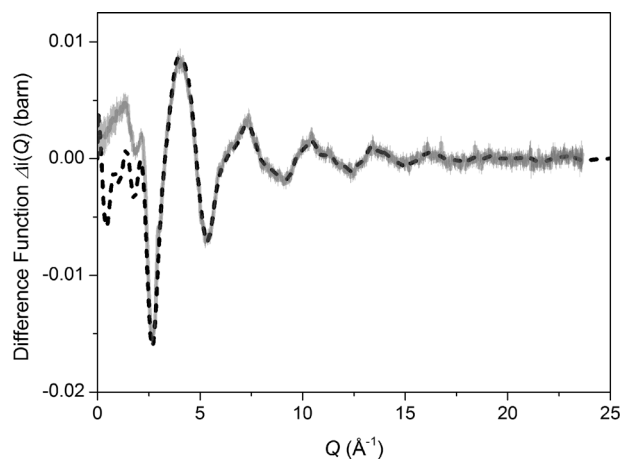

Fig. 3 First order difference function $\Delta i(Q)$ formed by $^{46}i(Q)$–$^{48}i(Q)$ (solid grey curve) and the corresponding back Fourier transform after the low-r oscillations of $\Delta T(r)$ have been removed (broken dark curve).

Table 1 Weighting factors w_{ij} calculated using eqn (12) and (13), (barn = 10^{-28} m^2)

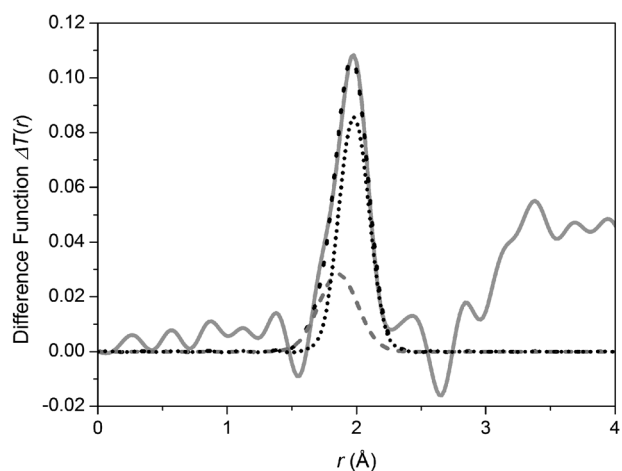|	$^{46}T(r)$		$^{48}T(r)$		$\Delta T(r)$	
	mbarn	%	mbarn	%	mbarn	%
$t_{Ti-O}(r)$	2.2	0.9	−5.3	2.1	7.5	64.4
$t_{Ti-Ca}(r)$	0.3	0.1	−0.7	0.3	1.0	8.5
$t_{Ti-Na}(r)$	0.4	0.2	−1.0	0.4	1.4	11.9
$t_{Ti-Si}(r)$	0.4	0.2	−1.1	0.4	1.5	12.9
$t_{Ti-P}(r)$	0.1	0.02	−0.1	0.1	0.2	1.8
$t_{Ti-Ti}(r)$	0.01	0.004	0.1	0.03	−0.1	0.5
$t_{Si-O}(r)$	41.8	16.5	41.8	16.2	0	
$t_{Si-Ca}(r)$	5.5	2.2	5.5	2.1	0	
$t_{Si-Na}(r)$	7.8	3.1	7.8	3.0	0	
$t_{Si-P}(r)$	1.2	0.5	1.2	0.5	0	
$t_{Si-Si}(r)$	4.2	1.7	4.2	1.6	0	
$t_{Ca-O}(r)$	27.6	10.9	27.6	10.7	0	
$t_{Ca-Na}(r)$	5.1	2.0	5.1	2.0	0	
$t_{Ca-P}(r)$	0.8	0.3	0.8	0.3	0	
$t_{Ca-Ca}(r)$	1.8	0.7	1.8	0.7	0	
$t_{Na-O}(r)$	38.7	15.3	38.7	15.0	0	
$t_{Na-P}(r)$	1.1	0.4	1.1	0.4	0	
$t_{Na-Na}(r)$	3.6	1.4	3.6	1.4	0	
$t_{P-O}(r)$	5.8	2.3	5.8	2.3	0	
$t_{P-P}(r)$	0.1	0.03	0.1	0.03	0	
$t_{O-O}(r)$	104.4	41.3	104.4	40.5	0	

Fig. 4 Real space data for the first order difference function $\Delta T(r)$ formed by Fourier transforming the difference function $\Delta i(Q)$ and the corresponding Ti–O fit. The solid grey curve represents the experimental difference function $\Delta T(r)$, the grey broken and black dotted curves represents 4 fold Ti–O at 1.86 Å and 6-fold Ti–O at distance of 1.98 Å respectively and the dark short dashed curve represent the fit (sum of the 4- and 6-fold Ti–O correlations).

neighbor Ti correlations such as Ti–(O)–Si, Ti–(O)–Ca, Ti–(O)–Na and Ti–(O)–P are not expected to appear until beyond 3 Å. In addition to the Ti–i correlations present, the Ti–O correlation now accounts for ~65% of the signal present in difference function $\Delta i(Q)$ (see Table 1). The real-space first order difference function, $\Delta T(r)$ was fitted using the *Matlab* program *NXFit*.[67] The area under the Ti–O correlation corresponds to an average coordination number of 5.2(1) oxygen atoms around Ti. Fig. 4 shows the resultant fit, the solid grey curve represents the experimental difference function $\Delta T(r)$, the grey broken and black dotted curves represents 4 fold Ti–O at 1.86 Å and 6-fold Ti–O at distance of 1.98 Å respectively, and the dark short dashed curve represent the fit (sum of the 4 and 6-fold Ti–O correlations). This corresponds to 60% (±5%) octahedral Ti–O and 40% (±5%) tetrahedral Ti–O.

These Ti–O distances are in reasonable agreement with previously published values given for 4-fold (1.83 Å) and 6-fold Ti–O (1.96 Å).[68–71]

The K-edge Ti XANES data is shown in Fig. 5. There is no noticeable variation in the data sets collected throughout the sample and macroscopic phase separation is not present on the 4 micron length scale made accessible by the focused X-ray beam. The presence of a pre-peak, *i.e.* at an energy below the main absorption edge, is consistent with there being a significant fraction of 4-fold (or 5-fold) coordinated Ti.[72] The relative height of the pre-peak, at ~0.4 of the overall edge step, excludes the possibility of the majority of Ti being in a 4-fold environment and indicates either a mixture of 4- and 6-fold Ti or the presence of 5-fold Ti. The XANES data is therefore consistent with the isotopic substitution neutron data.
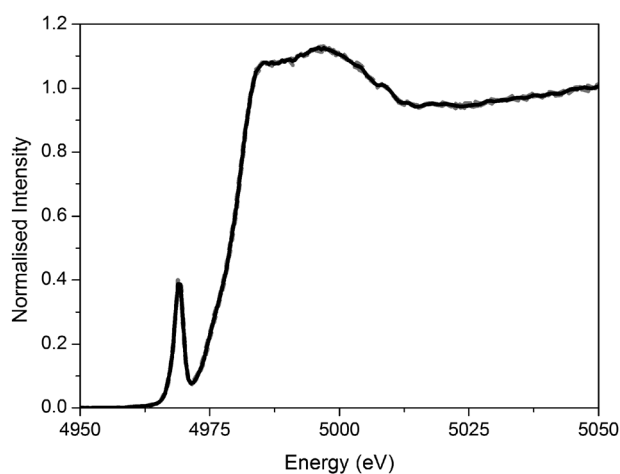
Fig. 5 Ti K-edge XANES for Ti Bioglass. The grey dashed lines show the individual data sets whilst the dark solid line shows the averaged data. The data sets are almost indistinguishable apart from the expected statistical variations.
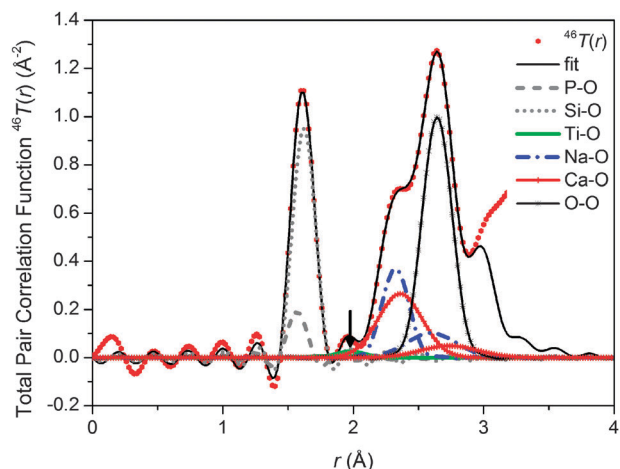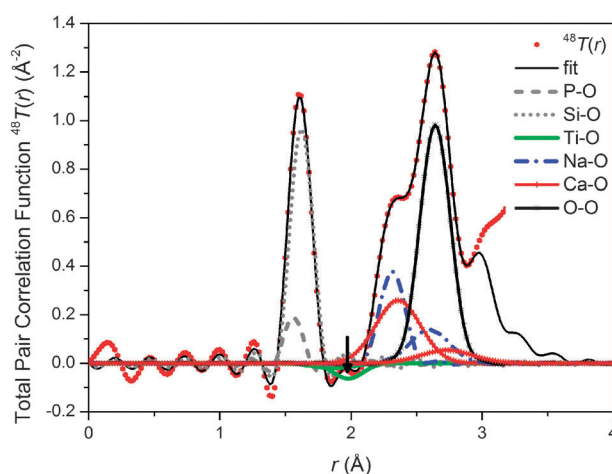

Fig. 7 Total correlation function $^{48}T(r)$, the optimum fit and selected partials. The Ti–O correlation is highlighted by the arrow. The Ti–O correlation is negative due to the negative coherent scattering factor of ^{48}Ti.

Table 2 Structural parameters for $^{46}T(r)$ and $^{48}T(r)$ obtained using the *NXFit* fitting routine. The parameters for 45S5 Bioglass $T(r)$ are included for comparison. Typical errors are ±0.02 Å on the peak position (r_{ij}), ±0.2 on the coordination number (n_{ij}) and ±0.02 Å on the disorder parameter (σ_{ij})

	$^{48}T(r)$			$^{46}T(r)$			Bioglass 45S5 $T(r)$		
	r_{ij}	n_{ij}	σ_{ij}	r_{ij}	n_{ij}	σ_{ij}	r_{ij}	n_{ij}	σ_{ij}
$t_{P-O}(r)$	1.59	4.0	0.01	1.57	4.0	0.01	1.60	4.0	0.01
$t_{Si-O}(r)$	1.62	4.0	0.08	1.62	4.0	0.07	1.62	4.0	0.08
$t_{Ti-O}(r)$	1.86	1.5	0.15	1.86	1.5	0.15			
$t_{Ti-O}(r)$	1.98	3.7	0.11	1.98	3.7	0.11			
$t_{Na-O}(r)$	2.33	3.1	0.12	2.34	3.1	0.12	2.33	3.1	0.15
$t_{Ca-O}(r)$	2.36	5.3	0.13	2.35	5.3	0.13	2.35	5.3	0.11
$t_{Na-O}(r)$	2.62	1.6	0.10	2.61	1.6	0.10	2.63	1.6	0.10
$t_{O-O}(r)$	2.66	4.0	0.11	2.66	4.0	0.11	2.65	4.0	0.11
$t_{Ca-O}(r)$	2.71	1.3	0.17	2.70	1.3	0.17	2.76	1.3	0.20

Fig. 6 Total correlation function $^{46}T(r)$, the optimum fit and selected partials. The Ti–O correlation is highlighted by the arrow.

Real space data for the total structure factors, $^{46}i(Q)$ and $^{48}i(Q)$, were fitted using the *NXFit* program.[67] The resultant fits for $^{46}T(r)$ and $^{48}T(r)$ are shown in Fig. 6 and 7 respectively and the optimum fit parameters are given in Table 2. Table 2 also presents the results of fitting Ti free 45S5 bioglass. These results were collected using the ISIS pulsed neutron source. Detail of the data analysis is given by Martin *et al.*[27] To enable a direct comparison with the present data the reciprocal data was truncated at a Q_{max} of 23.66 Å (to match the Ti bioglass data) before Fourier transforming into real-space and fitting using the *NXFit* analysis program.

The short range order comprise ∼4 oxygen atoms around Si at ∼1.62 Å and ∼4 oxygens around P ∼ 1.58 Å. Ti–O correlations account for the region 1.7 < r (Å) < 2.1 as determined from the first order difference function discussed above. The third structural region ∼2.2 to 2.9 Å contains overlapping O–(P)–O, O–(Si)–O, Ca–O and Na–O correlations making it challenging to deconvolve specific correlations from the real space total diffraction data. However, using the

network connectivity model discussed in Section 1.1. it is possible to estimate *a priori* the most probable O···O correlations: the O–(P)–O and O–(Si)–O are both tetrahedrally coordinated, therefore the expected O–(X)–O distance is given by $\sqrt{8/3}r_{X-O}$, where X represents P or Si. The concentration of Si is ∼10 times greater than the concentration of P; the O···O correlation can therefore be modeled using a single O···O correlation that is largely determined by the O–(Si)–O term. In the present system R = 0.4, giving Z = 1.0 (eqn (4)) and a network connectivity of 1.97 (eqn (1)). From the network connectivity it is possible to calculate the number of bridging oxygen atoms and therefore the O–(Si)–O coordination number. Each non-bridging oxygen atom is surrounded by 3 nearest neighbor oxygen atoms, whilst each bridging oxygen atom is surrounded by six nearest neighbor oxygen atoms. Assuming the glass contains only two distinct Q species; a network connectivity of 1.97 corresponds to 97% of the Si being Q^2 and the remaining 3% being Q^1. Thus the average coordination number of O–(Si)–O is expected to be 3.98.

Fig. 8(a) shows the ^{29}Si MAS NMR data characterizing this system. This ^{29}Si spectrum can be simulated using a single Gaussian line positioned at −80.5 ppm (see inset on Fig. 8(a)).
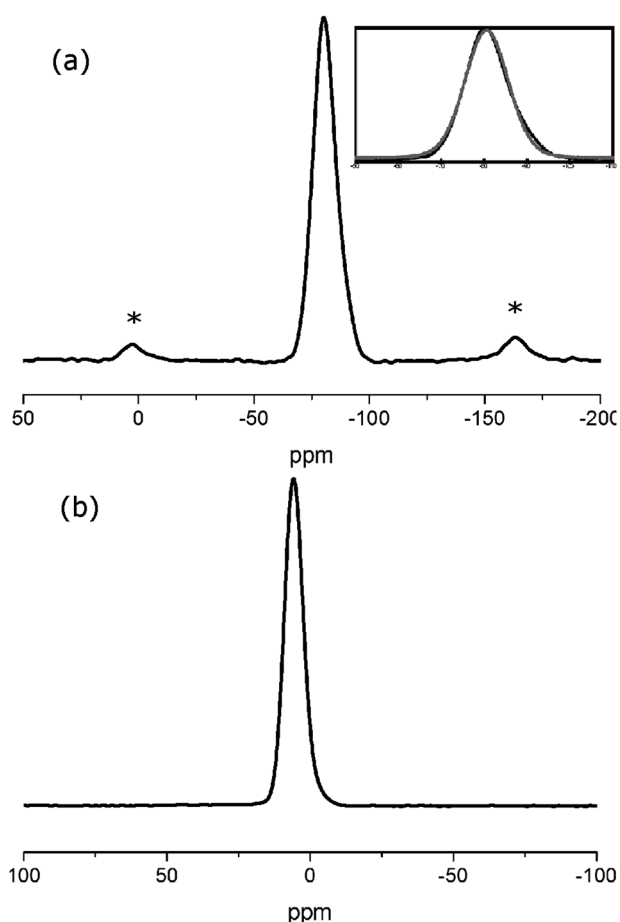
Fig. 8 (a) ^{29}Si and (b) ^{31}P NMR spectra. * indicates the spinning sidebands.

This result suggests that the Si speciation is clearly dominated by Q^2 structural moieties, and smaller quantities of other structural components such as Q^1 (at ~ -75 ppm) and Q^3 (at ~ -90 ppm) species are not observable at the $\sim 3\%$ level postulated in the proposed structural model above. The Q^2 species linewidth at half-height of 11.9 ppm (or ~ 700 Hz) causes significant spectral overlap with the corresponding Q^1 and Q^3 chemical shift regions and precludes their independent observation if they are present at low concentrations. The Q^2 chemical shift of -80.5 ppm is consistent with similar assignments in the range of -79.6 to -81.7 ppm reported in other bioglass systems.[73] Importantly, only the average Q^n species is required to calculate the O–(Si)–O coordination number given in the model. Fig. 8(b) shows the corresponding ^{31}P MAS NMR data for this bioglass system. This ^{31}P resonance can be simulated using a single Gaussian lineshape centered at 5.8 ppm; the line-width measured at half-height is 9.3 ppm (or 1.5 kHz). There are no resolved resonances or shoulders observed in the -3.0 to -4.4 ppm range corresponding to Q^1 P species; this is consistent with a previous study that reports a resonance located at ~ 5.8 ppm as assigned to Q^0 orthophosphate structural moieties.[73] Each oxygen atom is therefore surrounded by 3 nearest neighbor O–(P)–O. Thus by allowing 100% of the Si and 40% of the Ti to have an O···O coordination of 3.98 and 100% of the P and the remaining 60% of the Ti to have an

O···O coordination of 3, an overall O···O coordination number of 3.89 is expected. The O···O coordination for the present system is 4.0(1) which is in good agreement with the theoretical value based on the network connectivity of the glass with phosphorous being orthophosphate and 40% of the titanium entering the silicon network.

The Ca–O feature was modeled using two Ca–O distances based on recently obtained results for an analogous Ca/Sr bioglass system.[28] The values, determined for the Ti bioglass system, of 5.3(1) oxygens around Ca at 2.35(3)/2.36(3) Å and 1.3(1) oxygen atoms around Ca at 2.70(3)/2.71(3) Å are in good agreement with the previous reported values of 5.4 oxygen around Ca at 2.33 Å and 1.3 oxygen around Ca at 2.73 Å. It is also interesting to note that the Ca–O values presented for this melt quench system are in good agreement with experimental values reported in sol–gel derived $(SiO_2)_{70}(CaO)_{30}$ bioactive glasses where Ca–O_{NB} and Ca–O_B distances of 2.32 and 2.75 Å were reported.[74] The number of non-bridging oxygen atoms around calcium is also in excellent agreement with the molecular dynamics results (5.4) for melt quench glasses.[19] No Ca–OH correlations ~ 2.5 Å were observed as expected for a melt quench glass.

The Na–O feature was also modeled using two Na–O distances based on results recently obtained by the method of isomorphic substitution of a mixed Na/Li bioglass.[27] Furthermore, an asymmetric Na–O peak has also been reported both experimentally in sodium silicates and in molecular dynamic simulations on sodium calcium silicates and on Bioglass®.[75–78] The Na–O values of 3.1 oxygen around Na at 2.33 Å and 1.6 oxygen around Na at $\sim 2.62(2)$ Å obtained in this study are consistent with results cited above.[27]

It is not possible to model correlations beyond ~ 3 Å due to the large number of overlapping correlations such as Si–(O)–Si, Si–(O)–Ti, P–(O)–P followed by P–(O)–Na, P–(O)–Ca and so forth.

The molar ratio of $TiO_2 : SiO_2$ in the titanium doped bioglass has been kept constant, at 0.08 : 0.92, to avoid the risk of phase separation and to enable a direct comparison with the sol–gel titanium silicate previously studied.[42] It is interesting to note that the glass presented here shows predominantly 6-fold TiO_2, which is also what was observed in the precursor $TiO_2 : SiO_2$ sol–gel when calcined at lower temperatures but which contrasts with the predominantly 4-fold Ti coordination observed after heat treating to 500 °C or higher. This reduction in coordination presumably corresponded to the removal of OH groups (acting as modifiers) from the sol–gel. It is therefore postulated that the addition of modifiers, in the present case Na and Ca, strongly influence the local environment surround the titanium ions.

The network connectivity of Bioglass® is 2.11 as given in Section 1.1. The addition of 4 mol% of TiO_2 could in theory reduce the network connectivity to as low as 1.76 if the Ti was 100% 6-fold (noting that, if the network connectivity is too low, the glass dissolves too quickly and hydroxypatite does not have time to form – i.e. the bioactivity is effectively reduced). Alternatively, if the titanium is 100% 4-fold then the network connectivity would increase to 2.26 (noting that, if the network connectivity is too high, the glass does not release sufficient Ca and P for hydroxyapatite to form – reducing the bioactivity again).

For the present system 40% of the titanium was found to be 4-fold coordinated with the remaining 60% being 6-fold thus resulting in a network connectivity of 1.97. The addition of titanium has therefore decreased the network connectivity slightly compared to the titanium-free bioglass, a fact which is likely to reduce its chemical durability under physiological conditions, and thus alter the bioactivity of the glass. Whilst these results do not preclude the existence of some 5-fold coordinated titanium the results do place a maximum limit on the fraction of 4-fold present and therefore also sets an upper limit on the network connectivity. Knowledge of the Ti–O coordination will enable these systems to be better modeled. Furthermore, with this knowledge, and using the above network connectivity model it is now possible to alter the network modifier concentration in a controlled fashion in order to compensate for the effects of Ti and thus design Ti-bioglasses with a network connectivity equal to that of Bioglass® at 2.11.

4. Conclusions

Isotopic substitution applied to neutron diffraction has enabled the Ti–O coordination to be successfully isolated from the complex total structure factor. The titanium-doped Bioglass sample reported here, represents to the best of our knowledge, the most complex amorphous material (6 chemical elements and 21 partial structure factors) and the lowest level of isotopic enrichment (1.36 mol% Ti) ever studied using isotopic substitution for an amorphous system. Forming the first order difference function resulted in the subtraction of 98.7% of the total structure factor. Furthermore these samples contained 3 separate network formers (Si, P and Ti). The results show Ti occupies a range of environments with a maximum of 40% being tetrahedrally coordinated. This is in contrast to the tetrahedral environment Ti occupies in the high temperature sol–gel phase. The results in turn set an upper limit of 1.97 for the network connectivity of the glass. The connectivity therefore decreases upon the addition of small amounts of titanium dioxide which in turn aids the dissolution of the glass. XANES has confirmed that the Ti–O is not phase separated on the micron length scale.

The O···O pair correlation was successfully modeled on the basis on the theoretical network connectivity and confirmed by solid state NMR results. The modeled Ca–O and Na–O environments were consistent with the Ti-free bioglass and in good agreement with recently reported values obtained using the method of isomorphic substitution neutron diffraction on other oxide glasses.

Acknowledgements

References

1 L. L. Hench, R. J. Splinter, W. C. Allen and T. K. Greenlee, *Biomed. Mater. Symp.*, 1971, **5**, 25.
2 A. E. Clark, L. L. Hench and H. A. Paschall, *J. Biomed. Mater. Res.*, 1976, **10**, 161.
3 L. L. Hench, *J. Mater. Sci.: Mater. Med.*, 2006, **17**, 967.
4 L. L. Hench, W. June and D. C. Greenspan, *J. Australas. Ceram. Soc.*, 2004, **40**, 1.
5 A. A. Gorustovich, J. M. Lopez, M. B. Guglielmotti and R. L. Cabrini, *Biomed. Mater.*, 2006, **1**, 100.
6 D. C. Clupper and L. L. Hench, *J. Mater. Sci.: Mater. Med.*, 2001, **12**, 917.
7 E. A. Abou Neel, D. M. Pickup, S. P. Valappil, R. J. Newport and J. C. Knowles, *J. Mater. Chem.*, 2009, **19**, 690.
8 R. M. Moss, *et al.*, *J. Non-Cryst. Solids*, 2010, **356**, 1319.
9 Y. Minaberry and M. a. Jobbágy, *Chem. Mater.*, 2011, **23**, 2327.
10 I. Izquierdo-Barba, D. Arcos, Y. Sakamoto, O. Terasaki, A. López-Noriega and M. a. Vallet-Regí, *Chem. Mater.*, 2008, **20**, 3191.
11 J. Román, S. Padilla and M. Vallet-Regí, *Chem. Mater.*, 2003, **15**, 798.
12 D. Arcos, D. C. Greenspan and M. Vallet-Regi, *Chem. Mater.*, 2002, **14**, 1515.
13 P. Sepulveda, J. R. Jones and L. L. Hench, *J. Biomed. Mater. Res.*, 2002, **59**, 340.
14 V. FitzGerald, R. A. Martin, J. R. Jones, D. Qiu, K. M. Wetherall, R. M. Moss and R. J. Newport, *J. Biomed. Mater. Res., Part A*, 2009, **91A**, 76.
15 R. A. Martin, S. Yue, J. V. Hanna, P. D. Lee, R. J. Newport, M. E. Smith and J. R. Jones, *Philos. Trans. R. Soc., A*, 2012, **370**, 1422.
16 Y. Xiang and J. Du, *Chem. Mater.*, 2011, **23**, 2703.
17 A. Pedone, T. Charpentier, G. Malavasi and M. C. Menziani, *Chem. Mater.*, 2010, **22**, 5644.
18 A. Tilocca, A. N. Cormack and N. H. de Leeuw, *Chem. Mater.*, 2007, **19**, 95.
19 R. N. Mead and G. Mountjoy, *Chem. Mater.*, 2006, **18**, 3956.
20 J. M. Oliveira, R. N. Correia and M. H. Fernandes, *Biomaterials*, 2002, **23**, 371.
21 R. D. Rawlings, *J. Mater. Sci. Lett.*, 1992, **11**, 1340.
22 R. Hill, *J. Mater. Sci. Lett.*, 1996, **15**, 1122.
23 A. C. Hannon, J. M. Parker and B. Vessal, *Proceedings of the Symposium on the Structural Chemistry of Silicates*, 1993, vol. 27, p. 293.
24 M. Corno, A. Pedone, R. Dovesi and P. Ugliengo, *Chem. Mater.*, 2008, **20**, 5610.
25 A. Tilocca, *J. Mater. Chem.*, 2010, **20**, 6848.
26 V. FitzGerald, D. M. Pickup, D. Greenspan, G. Sarkar, J. J. Fitzgerald, K. M. Wetherall, R. M. Moss, J. R. Jones and R. J. Newport, *Adv. Funct. Mater.*, 2007, **17**, 3746.
27 R. A. Martin, H. L. Twyman, G. J. Rees, J. M. Smith, E. R. Barney, M. E. Smith, J. V. Hanna and R. J. Newport, *Phys. Chem. Chem. Phys.*, 2012, **14**, 12105.
28 R. A. Martin, *et al.*, *J. Mater. Chem.*, 2012, **22**, 22212.
29 N. Miyata, K. Fuke, Q. Chen, M. Kawashita, T. Kokubo and T. Nakamura, *Biomaterials*, 2004, **25**, 1.
30 E. A. Abou Neel, W. Chrzanowski and J. C. Knowles, *Acta Biomater.*, 2008, **4**, 523.
31 N. J. Lakhkar, *et al.*, *Acta Biomater.*, 2012, **8**, 4181.
32 A. Oliva, A. Salerno, B. Locardi, V. Riccio, F. Della Ragione, P. Iardino and V. Zappia, *Biomaterials*, 1998, **19**, 1019.
33 N. Hijón, M. Manzano, A. J. Salinas and M. Vallet-Regí, *Chem. Mater.*, 2005, **17**, 1591.

34 N. Hijón, M. V. Cabañas, I. Izquierdo-Barba and M. Vallet-Regí, *Chem. Mater.*, 2004, **16**, 1451.
35 C. Gabbi, A. Cacchioli, B. Locardi and E. Guadagnino, *Biomaterials*, 1995, **16**, 515.
36 E. Saiz, M. Goldman, J. M. Gomez-Vega, A. P. Tomsia, G. W. Marshall and S. J. Marshall, *Biomaterials*, 2002, **23**, 3749.
37 T. Kokubo, H. Kushitani, S. Sakka, T. Kitsugi and T. Yamamuro, *J. Biomed. Mater. Res.*, 1990, **24**, 721.
38 A. K. Varshneya, *Fundamentals of Inorganic Glasses*, 2006.
39 O. Yamamoto, K. Alvarez, T. Kikuchi and M. Fukuda, *Acta Biomater.*, 2009, **5**, 3605.
40 S. Areva, T. Peltola, E. Säilynoja, K. Laajalehto, M. Lindén and J. B. Rosenholm, *Chem. Mater.*, 2002, **14**, 1614.
41 L. Cormier, P. H. Gaskell, G. Calas and A. K. Soper, *Phys. Rev. B: Condens. Matter Mater. Phys.*, 1998, **58**, 11322.
42 D. M. Pickup, F. E. Sowrey, R. J. Newport, P. N. Gunawidjaja, K. O. Drake and M. E. Smith, *J. Phys. Chem. B*, 2004, **108**, 10872.
43 G. W. Wallidge, R. Anderson, G. Mountjoy, D. M. Pickup, P. Gunawidjaja, R. J. Newport and M. E. Smith, *J. Mater. Sci.*, 2004, **39**, 6743.
44 D. M. Pickup, G. Mountjoy, M. A. Roberts, G. W. Wallidge, R. J. Newport and M. E. Smith, *J. Phys.: Condens. Matter*, 2000, **12**, 3521.
45 D. M. Pickup, G. Mountjoy, G. W. Wallidge, R. Anderson, J. M. Cole, R. J. Newport and M. E. Smith, *J. Mater. Chem.*, 1999, **9**, 1299.
46 G. Mountjoy, D. M. Pickup, G. W. Wallidge, R. Anderson, J. M. Cole, R. J. Newport and M. E. Smith, *Chem. Mater.*, 1999, **11**, 1253.
47 G. Mountjoy, D. M. Pickup, G. W. Wallidge, J. M. Cole, R. J. Newport and M. E. Smith, *Chem. Phys. Lett.*, 1999, **304**, 150.
48 M. A. Holland, D. M. Pickup, G. Mountjoy, E. S. C. Tsang, G. W. Wallidge, R. J. Newport and M. E. Smith, *J. Mater. Chem.*, 2000, **10**, 2495.
49 M. A. Holland, D. M. Pickup, G. Mountjoy, S. C. Tsang, G. W. Wallidge, R. J. Newport and M. E. Smith, *Applications of Synchrotron Radiation Techniques to Materials Science V*, 2000, vol. 590, p. 77.
50 D. M. Pickup, F. E. Sowrey, K. O. Drake, M. E. Smith and R. J. Newport, *Chem. Phys. Lett.*, 2004, **392**, 503.
51 F. J. Zhang, M. W. A. Skoda, R. M. J. Jacobs, R. A. Martin, C. M. Martin and F. Schreiber, *J. Phys. Chem. B*, 2007, **111**, 251.
52 L. Ianeselli, F. J. Zhang, M. W. A. Skoda, R. M. J. Jacobs, R. A. Martin, S. Callow, S. Prevost and F. Schreiber, *J. Phys. Chem. B*, 2010, **114**, 3776.
53 L. L. Hench and I. Thompson, *J. R. Soc., Interface*, 2010, **7**, S379.
54 R. A. Martin, H. Twyman, D. Qiu, J. C. Knowles and R. J. Newport, *J. Mater. Sci.: Mater. Med.*, 2009, **20**, 883.
55 L. J. Skipper, F. E. Sowrey, R. Rashid, R. J. Newport, Z. Lin and M. E. Smith, *Phys. Chem. Glasses*, 2005, **46**, 372.
56 V. FitzGerald, D. M. Pickup, D. Carta, D. Greenspan and R. J. Newport, *Phys. Chem. Glasses: Eur. J. Glass Sci. Technol., Part B*, 2007, **48**, 340.
57 V. FitzGerald, D. M. Pickup, D. Greenspan, K. M. Wetherall, R. M. Moss, J. R. Jones and R. J. Newport, *Phys. Chem. Glasses: Eur. J. Glass Sci. Technol., Part B*, 2009, **50**, 137.
58 Z. Strnad, *Biomaterials*, 1992, **13**, 317.
59 M. D. O'Donnell, S. J. Watts, R. V. Law and R. G. Hill, *J. Non-Cryst. Solids*, 2008, **354**, 3554.
60 H. E. Fischer, P. Palleau and D. Feltin, *Physica B*, 2000, **276**, 93.
61 H. E. Fischer, G. J. Cuello, P. Palleau, D. Feltin, A. C. Barnes, Y. S. Badyal and J. M. Simonson, *Appl. Phys. A: Mater. Sci. Process.*, 2002, **74**, S160.
62 J. F. Jal, C. Mathieu, P. Chieux and J. Dupuy, *Philos. Mag. B*, 1990, **62**, 351.
63 M. A. Howe, R. L. McGreevy and P. Zetterstrom, *Computer Code CORRECT: Correction Program for Neutron Diffraction Data NFL Studsvik*, 1996.
64 G. J. Cuello, *J. Phys.: Condens. Matter*, 2008, **20**, 244109.
65 P. H. Gaskell, *Glasses and Amorphous Materials, Materials Science and Technology*, 9th edn, 1991, p. 175.
66 V. F. Sears, *J. Neutron Res.*, 1992, **3**, 26.
67 R. M. Moss, PhD Thesis, University of Kent, 2009.
68 http://www.cds.dl.ac.uk.
69 J. Kissel and R. Hoppe, *Z. Anorg. Allg. Chem.*, 1990, **582**, 103.
70 G. A. Lager, T. Armbruster, F. K. Ross, F. J. Rotella and J. D. Jorgensen, *J. Appl. Crystallogr.*, 1981, **14**, 261.
71 W. Gonschorek and R. Feld, *Z. Kristallogr.*, 1982, **161**, 1.
72 F. Farges, G. E. Brown and J. J. Rehr, *Geochim. Cosmochim. Acta*, 1996, **60**, 3023.
73 I. Elgayar, A. E. Aliev, A. R. Boccaccini and R. G. Hill, *J. Non-Cryst. Solids*, 2005, **351**, 173.
74 L. J. Skipper, F. E. Sowrey, D. M. Pickup, K. O. Drake, M. E. Smith, P. Saravanapavan, L. L. Hench and R. J. Newport, *J. Mater. Chem.*, 2005, **15**, 2369.
75 U. Hoppe, D. Stachel and D. Beyer, *Phys. Scr.*, 1995, **T57**, 122.
76 A. N. Cormack and J. C. Du, *J. Non-Cryst. Solids*, 2001, **293**, 283.
77 A. Tilocca, *J. Chem. Phys.*, 2008, **129**, 084504.
78 A. Tilocca and N. H. de Leeuw, *J. Mater. Chem.*, 2006, **16**, 1950.